Controlled Aggregation of Ferritin to Modulate MRI Relaxivity

Kevin M. Bennett,* Erik M. Shapiro,† Christopher H. Sotak,‡§ and Alan P. Koretsky*

*Laboratory of Functional and Molecular Imaging, National Institutes of Neurological Disease and Stroke, National Institutes of Health, †Department of Radiology, Yale University, New Haven, Connecticut; ‡Worcester Polytechnic University, Departments of Biomedical Engineering and Chemistry and Biochemistry, Worcester Massachusetts; and §University of Massachusetts Medical School, Department of Radiology, Worcester, Massachusetts

ABSTRACT Ferritin is an iron storage protein expressed in varying concentrations in mammalian cells. The deposition of ferric iron in the core of ferritin makes it a magnetic resonance imaging contrast agent, and ferritin has recently been proposed as a gene expression reporter protein for magnetic resonance imaging. To date, ferritin has been overexpressed in vivo and has been coexpressed with transferrin receptor to increase iron loading in cells. However, ferritin has a relatively low T_2 relaxivity ($R_2 \approx 1\ mM^{-1}s^{-1}$) at typical magnetic field strengths and so requires high levels of expression to be detected. One way to modulate the transverse relaxivity of a superparamagnetic agent is to cause it to aggregate, thereby manipulating the magnetic field gradients through which water diffuses. In this work, it is demonstrated by computer simulation and in vitro that aggregation of ferritin can alter relaxivity. The effects of aggregate size and intraaggregate perturber spacing on R_2 are studied. Computer modeling indicates that the optimal spacing of the ferritin molecules in aggregate for increasing R_2 is 100–200 nm for a typical range of water diffusion rates. Chemical cross-linking of ferritin at 12 Å spacing led to a 70% increase in R_2 compared to uncross-linked ferritin controls. To modulate ferritin aggregation in a potentially biologically relevant manner, ferritin was attached to actin and polymerized in vitro. The polymerization of ferritin-F-actin caused a 20% increase in R_2 compared to unpolymerized ferritin-G-actin. The R_2-value was increased by another 10% by spacing the ferritin farther apart on the actin filaments. The modulation of ferritin aggregation by binding to cytoskeletal elements may be a useful strategy to make a functional reporter gene for magnetic resonance imaging.

INTRODUCTION

Magnetic resonance imaging (MRI) has emerged as an important technology for the noninvasive assessment of biological tissue and has enabled the assessment of anatomical and physiological processes for research and clinical applications. Some advantages of MRI as an imaging modality are its lack of ionizing radiation, high spatial resolution, and flexibility in type of contrast mechanisms. MRI offers the advantage of whole-tissue penetration with high-resolution (hundreds of microns in each dimension) in a reasonable period of time. MRI also has been used to obtain information about molecular events in vivo (1–6).

There has been some interest in developing reporter protein strategies to use MRI to image gene expression. The large impact of green fluorescent protein and luciferase for optical imaging of gene expression makes it attractive to have an MRI reporter protein that would enable high-resolution imaging throughout an organ. A reporter gene is a DNA construct that enables cells to express a protein that changes the MRI signal. The expression of the protein can be linked to activity of a different promoter (7). There have been a number of demonstrations of magnetic resonance (MR) reporter proteins including creatine kinase and arginine kinase, transferrin receptor, and polyarginine peptides (7). None of these strategies has found widespread use. Recently, ferritin has been proposed as an MRI reporter protein. The presence and overexpression of ferritin, an iron storage protein, has been detected in vitro and in vivo using MRI (8–11). However, wild-type ferritin is a poor MR contrast agent, with per-iron relaxivity ~10- to 100-fold lower than similarly sized synthetic iron oxide particles used for cell labeling (12). Wild-type ferritin also has a low per-ferritin relaxivity due to the fact that ferritin usually fills to approximately one third to one half of its maximum iron capacity (13). Nonetheless, there are some characteristics of ferritin that potentially could be improved.

Ferritin has a magnetic moment that interacts with a strong magnetic field to produce a perturbation that is detectable with MRI (14–18). The electron spins of the ferritin iron atoms are antiferromagnetically coupled, but the relatively small size of the core creates a cooperativity of spins and results in a superparamagnetic molecule. In an MRI of samples containing suspensions of ferritin, transverse relaxation rates are increased with an increase in ferritin concentration. The longitudinal (R_1) and transverse (R_2) relaxivities of different ferritin types depend on the amount of Fe^{3+} in the core, field strength, and temperature (17). A goal of previous works has been to noninvasively quantify the amount of iron present in the liver, spleen, and other organs based on ferritin relaxivity (19,20). These measurements are useful for studying tissue damage due to iron storage diseases. The relaxivity of ferritin is on the order of 1–10 $mM^{-1}s^{-1}$ at typical magnetic field strengths in the range of 1–10 T. Although synthetic versions of ''magnetoferritin'' have been produced in vitro (21,22), it is not yet

Submitted June 26, 2007, and accepted for publication December 31, 2007.

Address reprint requests to Alan P. Koretsky, Laboratory of Functional and Molecular Imaging, NINDS Building 10, Room B1D728, 10 Center Dr., MSC 1065, Bethesda, MD 20892-1065.

Editor: Arthur G. Palmer III.

0006-3495/08/07/342/10 $2.00

doi: 10.1529/biophysj.107.116145

clear that the fundamental relaxivity of the native ferritin molecule can be increased in vivo.

Studies of the tissue distribution of ferritin have emphasized the fact that the spatial organization of ferritin can affect the apparent R_2. One way to modulate the relaxivity of a superparamagnetic molecule is to allow it to aggregate (23–26). Indeed, controlling the aggregation has been proposed as a method for creating functional MRI contrast agents (26–28). The goal of this work is to determine whether the relaxivity of ferritin could be manipulated by controlled aggregation and to measure the conditions required to optimize aggregation to modulate R_2. We developed a computational model of ferritin in aggregation states of varying size and spacing. The results indicate that ferritin molecules in aggregates are optimally spaced at ≈100 nm for peak R_2 relaxivity. To verify the findings of the model, we chemically cross-linked ferritin at close distance in vitro to study the change in R_2.

Furthermore, we demonstrate a way to achieve spacing on the order of 100 nm in vitro by allowing ferritin to bind to a biological structure that polymerizes and depolymerizes at the correct distance. Actin, which is known to polymerize and change its structure with changes in the intracellular and extracellular environment (29–32), represents a large fraction (≈5%) of the total cellular-expressed protein and may thus be an appropriate scaffold to bind to ferritin to create optimal spacing. Actin is a monomer that hydrolyzes ATP to form filamentous polymers in vivo. Actin is ubiquitous in mammalian cells; it forms the cytoskeletal scaffold with which the nucleus, membrane, and organelles interact. The actin cytoskeleton interacts with cell-surface receptors to allow for cytokine-mediated cell motility. MRI contrast agents have been developed to detect cell molecular events occurring on the timescale of actin polymerization (33). We examined whether ferritin cross-linked to actin in vitro could be used to space ferritin at large distances and affect R_2. The results indicate that ferritin relaxivity can be modulated by polymerization of actin, which opens up the possibility of creating a ferritin–actin binding protein fusion that can report on the functional state of actin in cells.

MATERIALS AND METHODS

Theoretical simulations

A computational model was created (Microsoft Visual C++, version 6.0, Microsoft, Redmond, WA) to predict the MRI signal amplitude arising from water in a solution containing either disperse or aggregated perturbers. The overall scheme of the simulation was similar to that developed by Weisskoff et al (23) to study the effects of microscopic spherical perturbers on MRI relaxation. In this work, however, we looked at the effects of submicron perturber geometries and clustering on the MRI signal. Additionally, we developed a simulation of a Carr-Purcell Meiboom-Gill MRI pulse sequence, using a fixed diffusion time.

Spherical dipole perturbers were distributed randomly inside a simulated voxel volume with 10 μm in each of three dimensions. The perturber concentration was 6.1 nM (corresponding to a ferritin subunit concentration of ~145 nM), and the perturbers were not allowed to overlap. Each perturber was given a surface field offset of 20 G. An 11.7-T magnetic field was assumed. A water molecule, assumed to be infinitely small, was then placed within a smaller volume (100-nm isotropic) inside the center of the simulated voxel and allowed to diffuse through the 10 μm^3 isotropic voxel. To simulate the effects of perturber aggregation on the MR signal, a single perturber was placed at a random location, and then a specified number of perturbers were placed at fixed locations around it to form a cube. The spacing between individual perturbers was varied, as was the number of perturbers in each of the clusters, but the total number of perturbers in the simulated volume was held constant.

To simulate a multiple-echo (Carr-Purcell Meiboom-Gill) experiment, an echo-time (TE) was specified, and the water underwent a three-dimensional random walk through the field of perturbers during TE at a rate of 10,000 steps per second. Before each step, a random angle between each of three axes was computed to determine the direction of the next step, and water was not allowed to penetrate the perturbers. The effective diffusion coefficient based on empirical calculation of the RMS diffusion distance of water over TE was 4.24×10^{-4} mm^2/s, or ≈ 1/5 the diffusion coefficient of free water. After each step, the magnetic field at the location of the water molecule was calculated by adding the field contributions from every perturber at the location of the water. The phase was reversed five times to simulate five echoes, and signal intensity was calculated between each echo. We note that this would simulate an instantaneous 180° pulse, which is impossible in experiment. The perturbers were redistributed before each water molecule was placed in the field to randomize the spatial distribution of the perturbers. The total phase of the water molecule, which was the accumulated sum of the frequencies during the whole TE, was stored. This process was repeated for a total of 10,000 water molecules with a varying number of perturbers. The measurements of signal intensity with these parameters were accurate to $<1\%$, as long as the normalized signal intensity was >0.1. The measurements were all made in this range.

Chemical cross-linking of ferritin

To establish whether short-distance aggregation of ferritin could increase per-iron relaxivity in vitro, we created ferritin aggregates that were cross-linked at short distances. Iron concentrations of all stock ferritin samples used in this work were obtained from West Coast Analytical Service, Santa Fe Springs, CA. Cationized horse spleen ferritin (CF), a polycationic derivative of horse spleen ferritin, was obtained from Sigma (St. Louis, MO). To construct CF, the carboxyl groups of ferritin were activated by the manufacturer with a water-soluble carbodiimide and then reacted with N,N dimethyl-1,3 propanediamine to introduce free amine groups to the CF (34). Based on the electrometric titration of CF by Danon et al. (34), CF contains ~80–100 added free amine groups per ferritin cage.

We used 3,3′-dithiobis(sulfosuccinimidylpropionate) (DTSSP; Pierce, Rockford, IL) to cross-linked CF. DTSSP is a soluble succinimidyl ester containing a disulfide bond that links binding sites to two free amines. DTSSP forms a 12 Å (0.1 nm) spacer between neighboring cross-linked proteins. The structure of DTSSP is shown in Fig. 1 *a*, with binding sites for the ferritin subunits indicated by arrows.

The DTSSP cross-linking reaction was performed in phosphate-buffered saline (PBS), and 2-amino-2-hydroxymethyl-1,3-propanediol (TRIS) competitively inhibited the reaction. In addition, cross-linking with DTSSP was reversed using dithiothreitol (DTT), which reduces (cleaves) the disulfide bond between the DTSSP cross-linkers. Before use, the DTSSP was mixed with PBS at a 10 mg/mL concentration and put into solution by vigorous vortexing.

The experimental design for the ferritin aggregation experiments is shown in Fig. 1 *b*. In cross-linked and control experiments, respectively, CF was mixed with 0.9 mL PBS or 0.9 mL TRIS buffer (pH 7.4, 1 M) in concentrations from 50 nM to 500 nM (CF cage polymers). In both cross-linked and control samples, the DTSSP-PBS solution was added and thoroughly mixed by pipetting. After 1 h, 0.9 mL of TRIS was mixed by pipette with the cross-linked samples, and 0.9 mL of PBS was mixed with the control samples, making the total volumes (and ferritin, TRIS, and PBS concentrations) of the cross-linked and control samples the same. Thus, any differences in the MR

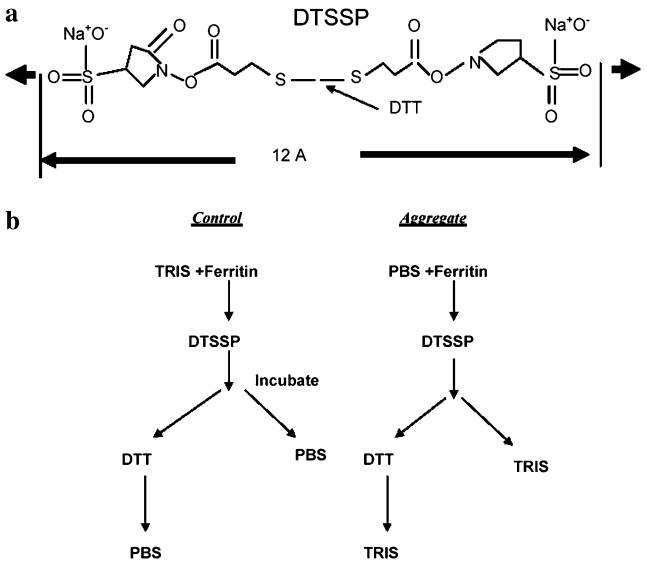

FIGURE 1 (*a*) The short (12 Å; 1 nm) spacer succinimidyl ester DTSSP was cross-linked on either side to an amine group on cationized horse-spleen ferritin. The thick arrows at left and right show the location of the ferritin attachment. The spacer was cleaved by DTT at the location of the thin arrow. (*b*) Illustration of experimental protocol for ferritin aggregation with DTSSP. Volumes of buffers were equal between control and aggregate samples. Aggregation was controlled by the addition of free amines in the form of TRIS buffer either before (control) or after (aggregate) cross-linking.

properties between cross-linked and control samples should be due only to the time allowed for aggregation to occur before the TRIS was added. The samples were then mixed 1:1 with 2% molten low-melting point agarose (SEAChem, Madison, GA.), at ~40°C, in glass test tubes and allowed to cool for 1 h at room temperature before imaging. To determine whether reversal of cross-linking could reverse any change in R_2 with aggregation, we added 50 μL of 10 mg/mL DTT to 900 μL of the cross-linked samples and 900 ul of the control samples. The experiments were repeated three times using separate cross-linked samples and control samples. The aggregate size distribution for the conditions of these experiments was determined by electron microscopy (described below).

Actin-ferritin conjugation and actin polymerization

As described in the Results section, the computer simulations predicted a dependence of ferritin relaxivity on the spacing between individual ferritins in the aggregate. To explore this effect in vitro and to make a biologically relevant construct of aggregated ferritin, we attached ferritin to actin and allowed actin polymerization to determine the spacing of the ferritin molecules.

Biotinylated rabbit skeletal muscle actin and all actin buffer solutions were purchased from Cytoskeleton, Inc. (Denver, CO). Avidin-ferritin, composed of horse-spleen ferritin conjugated to avidin (EY Laboratories, Inc., San Mateo, CA), was used. We added 2 μL of dH_2O and 48 μL of general actin buffer (5 mM Tris, 0.2 mM $CaCl_2$, and 0.2 mM ATP) to 2 μg of dehydrated biotin-actin and incubated for 1 h at room temperature.

To determine whether actin-ferritin could polymerize, 100 μL of avidin-ferritin (5 mg/mL) or general actin buffer was added to 20 μL of the biotin-actin solution, and the samples were incubated 30 min at room temperature. We added 12 μL of polymerization buffer (500 mM KCl, 20 mM $MgCl_2$, and 10 mM ATP) 1 h before, or directly before, suspension in 2% molten agarose in dH_2O (Bioline USA Inc., Randolph, MA) for transmission electron microscopy (TEM), or left it in solution for MRI. The concentration of ferritin cages was 3.5 μM. Hereafter, globular actin (G-actin) refers to unpolymerized actin, and F-actin refers to actin incubated with polymerization buffer for 1 h.

To modulate R_2 by modifying the spacing between each of the ferritin molecules, we mixed biotin-actin with rhodamine-actin in proportions of 1:1.5 and 1:5, then allowed the avidin-ferritin to conjugate with the mixture before polymerization (as described above). This should allow only some of the ferritin to be attached to F-actin thus increasing the overall distance between the ferritin cages. The samples were observed under electron microscopy (see below, with samples prepared by adsorption to the carbon grid).

Fluorescence microscopy

Actin, both ferritin-conjugated and by itself in G- and F-forms, was incubated with a rhodamine-phalloidin (Cytoskeleton) conjugate for fluorescence microscopy, which was performed using a Leica MZ FLIII stereo microscope with a TRITC/DiI filter (excitation 540 nm, emission 605 nm; Chroma Technology Corp, Rockingham, VT). For imaging, 10 μL of the actin sample was dropped onto a microscope slide and covered with a cover slip.

Electron microscopy

All images were taken with a Jeol electron microscope (JEM-200CX; Peabody, MA). For embedded samples of cross-linked and actin-conjugated ferritin, these solutions were mixed with 10% agarose. Cacodylate buffer was added to the agarose sample in a test tube and stored at 4°C. Selected areas were trimmed, dehydrated with a graded series of ethanol mixtures, infiltrated with graded mixtures of ethanol and epoxy resin (SPI Supplies, West Chester, PA), and embedded in epoxy resin. Polymerization of the resin was carried out at 60°C for $\leq$ 48 h. For carbon-grid adsorption, samples were adsorbed onto 400 hexagonal mesh, thin bar Cu grids (EMS, Fort Washington, PA) coated with 1% Formvar in ethylene dichloride (EMS) by settling for 5 min, and blotting and drying for 15 min. Separate grid-adsorbed samples were then negatively stained with 0, 0.25%, and 0.5% uranyl acetate in water.

Two different preparations of actin-ferritin were prepared for the cross-linked and control conditions. In the first, cross-linked and control samples were mixed 1:1 with 10% low-melting point agar and allowed to cool. In one of the samples, containing no ferritin, 0.5% uranyl acetate in 0.1 M acetate buffer was added to the section to provide negative contrast and to enable visualization of the actin filaments. Experiments were repeated three times with similar results.

Ferritin was easily identified with no negative staining and appeared to be arranged in filaments. Additionally, F-actin filaments were identified with uranyl acetate staining, but it was difficult to obtain sufficient contrast to identify actin and ferritin together due to absorption of uranyl acetate by the agar. The samples were therefore adsorbed onto carbon grids, as described above.

MRI

Samples of the chemically cross-linked ferritin in agar were imaged in 1.5 mL Eppend (Sigma Aldrich, St. Louis, MO) or 200 μL tubes and placed in a 35 mm ID Bruker transmit/receive probe in a Bruker 11.7T scanner (Bruker Biospin, Billerica, MA) with a 31-cm bore magnet (Magnex Scientific, Oxford, England). For T_2 mapping, a multishot multiecho pulse sequence was used (TE/TR = 6/3000 ms). Five slices of 0.5-mm thickness were acquired with 0.5 mm between each slice. In-plane resolution was 200 $\times$ 200 μm using a 128 $\times$ 128 matrix with a 25.6-mm^2 field of view.

Actin was imaged in solution. We used a custom-built, 55 mm ID transmit/receiver radiofrequency coil that allowed the samples to remain upright. All imaging parameters were the same as with the chemically cross-linked samples.

RESULTS

Simulations

In simulations of the MRI signal intensity using a single-voxel approach, ferritin-sized perturbers were randomly distributed in the pixel. The perturbers were allowed to aggregate with 2, 3, 4, or 5 perturbers in each dimension with no spacing between the perturbers. The space between the edges of the perturbers was also varied from 50 nm to 500 nm, and the MRI signal intensity was compared between the perturber orientations.

Fig. 2 *a* shows a typical plot of the simulated MRI signal intensity (on a negative log scale) as a function of *TE*, at each echo, for a zero-distance perturber spacing, with the number of perturbers in the aggregate varied from 8 ($2 \times 2 \times 2$ perturbers) to 125 ($5 \times 5 \times 5$ perturbers). Relaxivity was estimated by the slope of each curve. Fig. 2 *b* shows the resulting change in R_2 compared to the case of close-packed, (0 nm), aggregate of the same number of perturbers. Fig. 2 *c* shows the same data compared to the case of randomly distributed ferritins. The simulation shows that increasing the distance between ferritins in varying size aggregates can cause an increase in R_2 by $\leq$60% compared to an aggregate with no space between ferritins. In comparison to randomly distributed ferritins, aggregation can either increase or decrease R_2 depending on the ferritin spacing. This effect is assumed to come from the transition of the relaxivity between static-dephasing and diffusion-limited regimes when ferritin spacing is modulated (23). The peak relaxivity in this case occurred with 64 perturbers, corresponding to a perturber diameter of ~500 nm. The greatest gain in R_2 was achieved when aggregate size was modulated in the range of 50–100 perturbers.

We examined whether the sensitivity to aggregate size was due to the fact that, when more ferritins are in an aggregate, a water molecule may not experience the magnetic field of the cluster during the random walk. We therefore compared the magnetic field offsets at the locations of several water molecules during the walk. All water molecules were found to experience at least 1 magnetic field offset due to the perturbers during the random walk (data not shown).

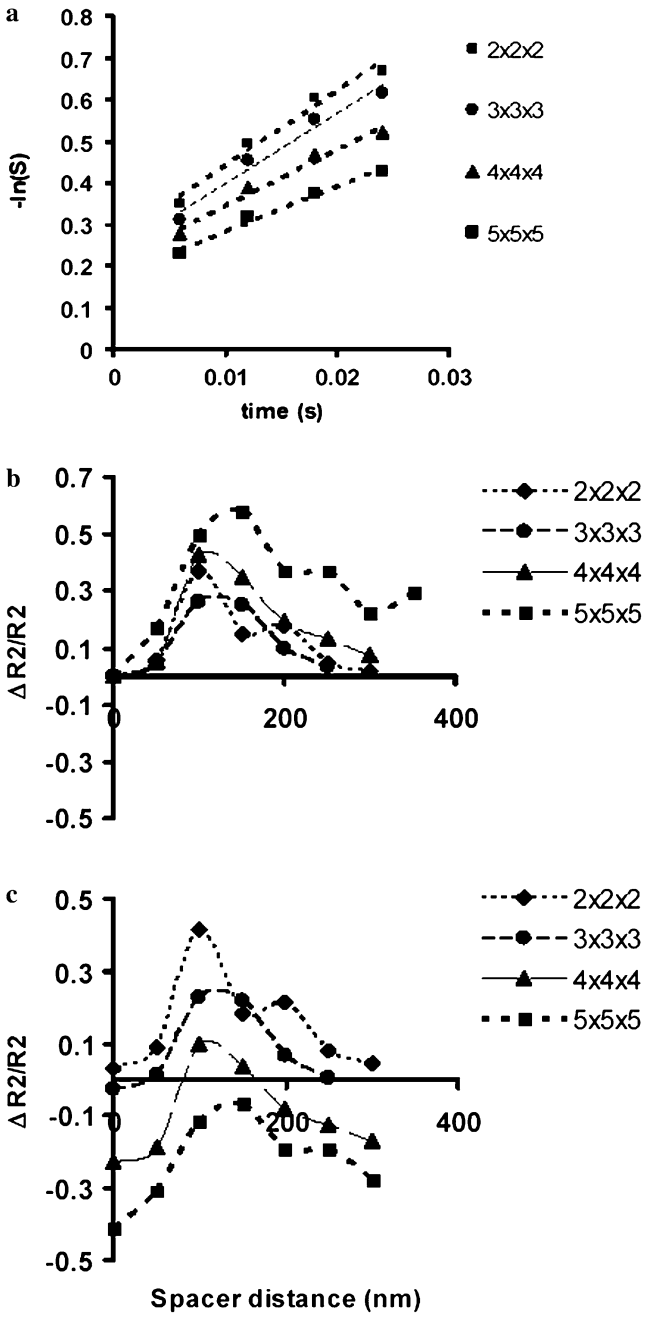

FIGURE 2 Simulation of the effects of aggregate size and perturber spacing on MR signal intensity with a CPMG (multiple-echo) pulse sequence with 4 ms TE. (*a*) Signal attenuation is shown to increase with the number of perturbers in the aggregate. (*b*) R_2 changes are shown for each aggregate size compared to the case of zero-length aggregation of the same number of perturbers. Peak relaxation occurred at a spacer distance of 100–150 nm for every aggregate. (*c*) The same data are shown compared to the case of randomly distributed perturbers in the voxel. With larger aggregate sizes, R_2 decreases due to shielding of the diffusing water from the central perturbers.

Chemical cross-linking of ferritin

Ferritin aggregates were observed in cross-linked samples using TEM with no negative staining. The spatial distribution of grid-adsorbed normal and aggregated ferritin is shown in Figs. 3, *a* and *b*, respectively. The distance across the large aggregates was measured to be ~150 nm on average, measured by the longest axis across embedded aggregates. The distribution of aggregate sizes for aggregated and native ferritin is shown in Fig. 3 *c*.

The MRI signal intensity in cross-linked and control samples decreased with increasing ferritin concentration. Typical MR images are shown in Fig. 4 *a*, with increasing concentrations of ferritin. The sample of aggregated ferritin was visibly darkened in T2-weighted images (TE = 36 ms) compared to controls. R_2 values, determined by fitting the signal decay with a monoexponential function, were used to

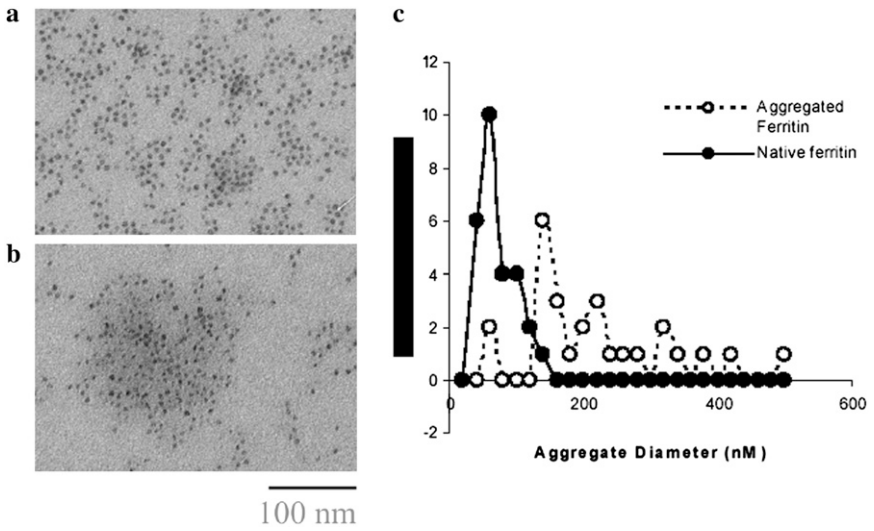

FIGURE 3 TEM images of (*a*) native horse spleen ferritin and (*b*) aggregated ferritin, cross-linked at short distance with DTSSP. Ferritin cages are visible as electron-dense dots in the image. (*c*) The aggregate diameter was estimated to be ~200 nm, corresponding to 20 ferritins in the longest dimension. Spontaneous aggregation of native ferritin was also observed, with an average aggregate diameter of ~75 nm.

compute relaxivity (per iron). The computed R_2-values are seen in Fig. 4 *b*, corresponding to the ferritin concentrations used in the samples of Fig. 4 *a*. The values of R_2 relaxivity, obtained by linear regression of the curves of Fig. 4 *b*, are shown in Fig. 4 *c*. Cross-linking of ferritin increased R_2 relaxivity by 70%, which was statistically significant ($p < 0.05$, *t*-test). The addition of DTT to reduce the disulfide linker caused relaxivity to decrease to the level of the control.

From these results, we concluded that chemical cross-linking of ferritin at short distances can increase R_2 relaxivity. This leads to a decrease in MRI signal intensity that is detectable at reasonable ET-values (10–40 ms) at high-field strengths. Additionally, the effect of cross-linking on R_2 relaxivity can be reversed by cleavage of the cross-linker.

Actin-ferritin conjugation and actin polymerization

To increase ferritin spacing to distances approaching 100 nm, we used polymerized actin as a scaffold for ferritin binding. The polymerization of actin in vitro was confirmed by fluorescence microscopy using rhodamine-phalloidin. No structured fluorescence was observed with G-actin samples (Fig. 5 *a*), whereas filaments of F-actin were seen (Fig. 5 *b*). The size of the filaments was on the order of 10–100 μm in length. G- and F-actin conjugates of ferritin were visible in TEM after adsorption to the carbon grid (Fig. 5, *c* and *d*), confirming that F-actin could still polymerize when ferritin was attached. F-actin was also visible in TEM of an agarose-embedded sample. Uranyl acetate staining provided excellent contrast of unpolymerized ferritin-actin and polymerized actin filaments in the agar (Fig. 5, *e* and *f*). The iron cores of individual ferritin molecules attached to polymerized actin were visible in TEM with no counterstain in agar blocks (Fig. 5 *f*). In this experiment, the close spacing of the individual ferritins was expected, because the ferritin concentration was equal to the actin concentration, and the ferritin molecules were separated by 5 nm. Filaments were ~200 nm in length and 5–10 nm in width. No filaments were observed in the G-actin sample, but there was some aggregation of ferritin-G-actin in grid-adsorbed samples, as seen in Fig. 5 *c*.

To determine whether an increased space between ferritin molecules in the aggregates could be used to modulate R_2, we used a 1:1.5 or 1:5 ratio of biotin actin to nonbiotin- (rhodamine-) actin in the samples. Fig. 6 *a* shows TEM images of these samples at two different magnifications. At constant ferritin concentrations, the spacing between ferritin iron cores in and around the aggregates increased from ~10 nm to 20–60 nm. There were more ferritins outside of the aggregates in the sample with a 1:5 ratio of biotin to nonbiotin actin, and there was a heterogenous distribution of spacing and aggregate sizes within the sample.

Fig. 6 *b* shows the values of R_2 for G- and F-actin, and for different concentrations of biotinylated actin, as obtained by fitting the signal attenuation curves for each sample. R_2 increased by 23% with actin polymerization, and the difference was significant ($p < 0.05$). The value of R_2 also was significantly higher between the 1:1.5 samples and the 1:5 samples of G-actin

We concluded that ferritin can be conjugated to actin in vitro and that the ferritin-actin conjugates are observable under electron microscopy. The polymerization of ferritin-conjugated actin can be detected with MRI by its effect on R_2, and this effect can be modulated by changing the space between ferritins.

DISCUSSION

In this work, we studied how the aggregation of ferritin can affect R_2 in MRI measurements. Aggregation is known to affect the relaxivities of superparamagnetic particles (26), and here we calculated the effects of size and interparticle spacing on the relaxivity of a model for ferritin. To the best of

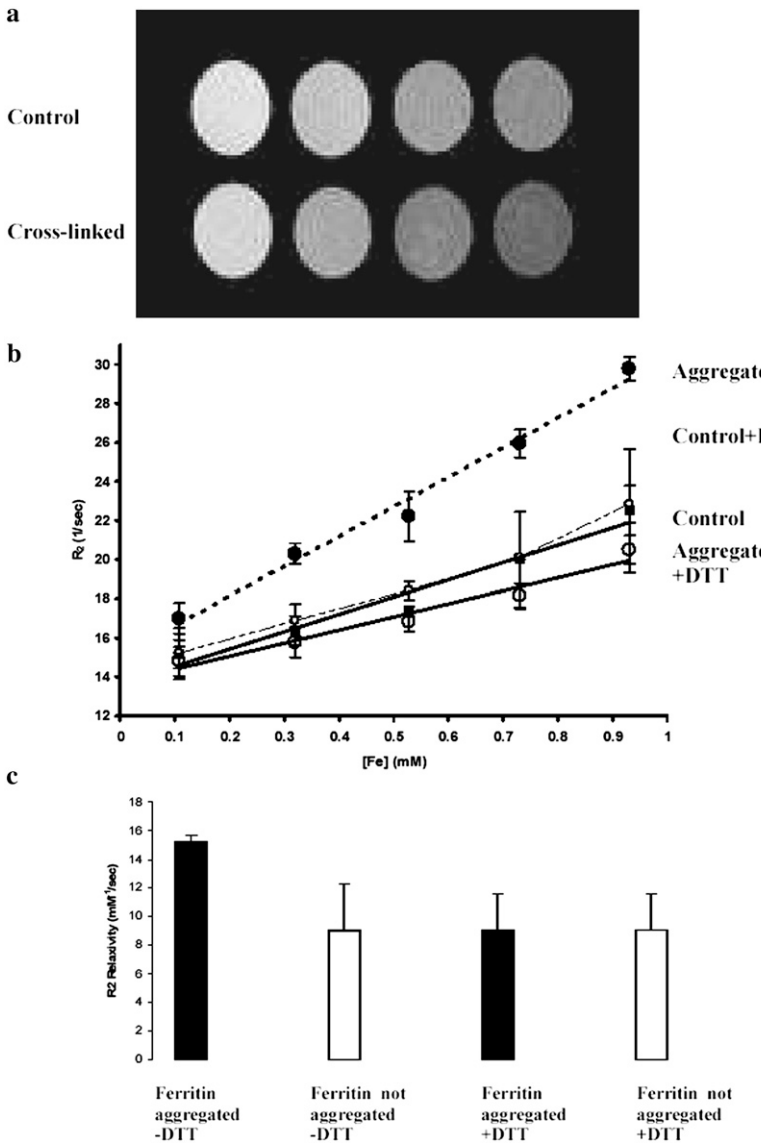

FIGURE 4 (*a*) Short-length cross-linking of cationized ferritin reduces MRI signal compared to uncross-linked controls. The images were taken with a CPMG pulse sequence with TE/TR = 6/3000 ms. The samples were embedded 1:1 in 2% agarose. (*b*) Effects of cross-linker (DTSSP) concentration on apparent R_2 of ferritin aggregates. The increase in R_2 with ferritin aggregation was reversed by cleaving the cross-linker with DTT. (*c*) Aggregation of ferritin increases per-iron R_2 relaxivity by 70%, as measured by CPMG MRI. The DTT was added to reverse cross-linking.

our knowledge, this is the first time the effects of interparticle spacing have been examined.

We used a computational model to study the change in relaxation rates for a number of perturber cluster sizes and interperturber spacings in spin-echo experiments. Qualitatively, the change in relaxation rates with perturber cluster size were in agreement with Weisskoff et al. (23) when the perturbers were touching. R_2 increased with cluster size, indicating that relaxation was diffusion limited at these perturber sizes. When the space between perturbers in the aggregates was increased, the maximum R_2 also increased. Based on the simulated results, a perturber spacing of 100–250 nm resulted in the largest ΔR_2. The optimal aggregate size was ~60–100 perturbers. To control for the effect of variations in the iron-loading factor in ferritin on the maximum ΔR_2, we also simulated the case where the surface-field offset was an order of magnitude greater (data not shown). Although the maximum ΔR_2 could be modulated in this way, the perturber sizes and spacing to achieve maximum ΔR_2 were approximately the same. Whereas the simulations are for superparamagnetic clusters, they are relevant for paramagnetic clusters and may explain the large relaxation detected in nanostructures such as gadolinium-doped carbon nanostructures (35). Our work demonstrates that it is feasible to rationally modify the distance between ferritin in a synthetic or endogenous contrast agent to modulate relaxivity, which is consistent with previous work with dextran-coated iron oxide particles (36).

To experimentally verify the trends predicted by the model, ferritin was cross-linked at short distances and bound to actin to cluster at larger distances. Cross-linking ferritin at short spacing increased R_2 by 70%, from 9 $mM^{-1}s^{-1}$ to 16 $mM^{-1}s^{-1}$. The value of 9 $mM^{-1}s^{-1}$ for unaggregated ferritin is within the range previously reported (12). Binding

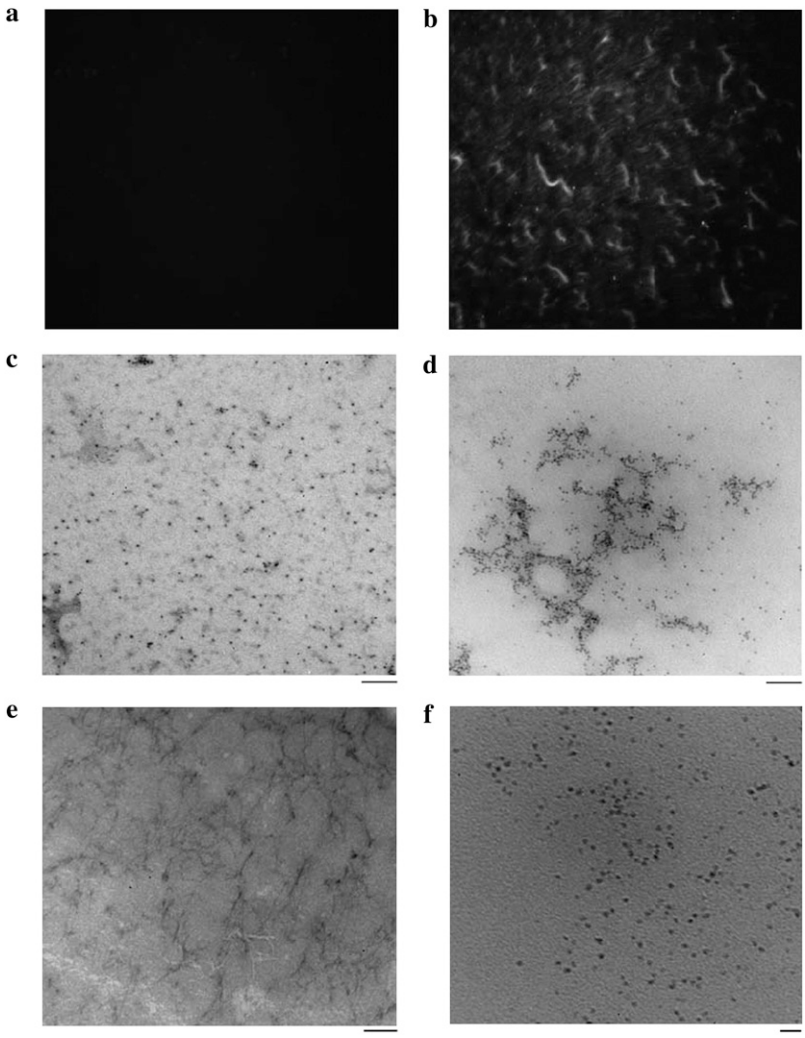

FIGURE 5 (*a* and *b*) Fluorescence microscopy (20× magnification) of rhodamine-conjugated phalloidin incubated with G-actin and F-actin, respectively. The samples in solution were imaged on a microscope slide using a TRITC/DiI filter (excitation 540 nm, emission 605 nm). Transmission electron micrographs of (*c*) ferritin-G-actin conjugates and (*d*) ferritin-F-actin conjugates adsorbed to a carbon mesh, demonstrating in vitro polymerization of actin-ferritin. Scale bars are 100 nm. (*e*) Transmission electron micrographs of ferritin-F-actin conjugates embedded in 10% agar with 0.5% uranyl acetate. Scale bar is 100 nm. (*f*) At higher magnification, with no stain, individual ferritins are observed attached to the actin. Scale bar is 20 nm.

ferritin to actin and increasing the ferritin spacing to ~50 nm increased R_2 by 30%.

Because the magnetic field offset from B_0 decreases as the cube of distance from the center of a perturber, it follows that the magnetic field 6.5 nm (2 × r) from a ferritin molecule is 12.5% of the value at the surface. At 19.5 nm (3 × r) away, the field offset drops to 3.7%. With three-dimensionally symmetric aggregation, the gradient is less steep. For instance, if the radius of the aggregation sphere is twice that of the single ferritin, the magnetic field offset is 67% at 6.5 nm and 40% at 19.5 nm. Thus, as the aggregate size increases, (assuming a zero-length spacer), the field perturbation is accessible to more of the water, but the size of the perturbing field gradient is reduced. Because the magnetic field gradient is responsible for dephasing, the goal in improving relaxivity via aggregation is to ensure that water is exposed to the field gradient as often as possible during the experiment. Both the effect of aggregating at short distances and altering interparticle spacing within aggregates can change R_2. The complexity of all of the factors involved makes it necessary to perform simulations, as we have here, to help optimize their effects.

Inner-sphere effects are known to affect the T_2 relaxivity of ferritin (18). It is thought that water adsorbed to the surface of the ferritin core is in rapid exchange with the bulk water, which adds to the intrinsic T_2 of ferritin in solution. However, aggregation of ferritin is not expected to decrease exchange of protons at the surface with the bulk water. Additionally, as noted above, the long-range magnetic field gradient induced at the core surface from a neighboring ferritin core, even when aggregated, is much smaller than at the surface. The effects of aggregation on relaxation are thus thought to come from outer-sphere mechanisms.

An alternative explanation for the relaxivity change with ferritin aggregation is that water becomes trapped between ferritins inside the aggregates. Trapped water would substantially increase the phase accumulation of water in the aggregates by forcing them to be in the vicinity of the dipolar fields of the ferritin molecules. In the simulations, this effect seems unlikely because, even with the largest aggregates, the volume of the aggregate only comprises ≈0.3% of the total volume of the simulated voxel. In experiments with actin-ferritin conjugates, this effect seems unlikely in the bulk

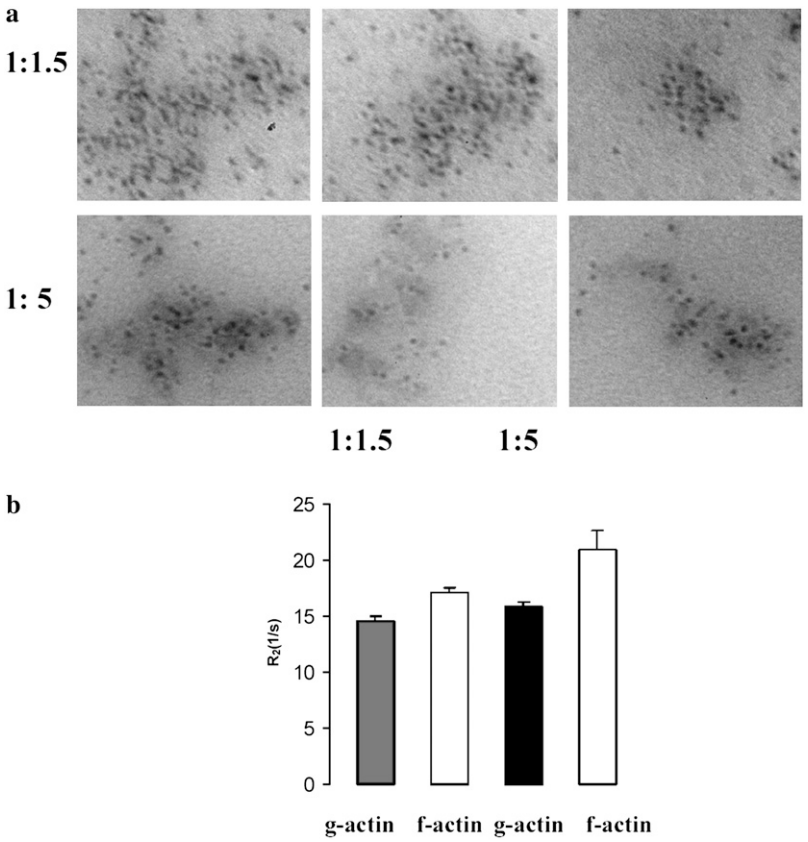

FIGURE 6 (*a*) Transmission electron micrographs of ferritin-F-actin conjugate in vitro, with two different ratios of biotin-actin to rhodamine-actin (1:1.5 and 1:5). Three of each sample are shown in a row. Samples were adsorbed on a carbon grid. Ferritin is visible as punctuate dark spots surrounding the negatively stained G- and F-actin. The F-actin samples with a 1:5 ratio had an increased distance between ferritin cores, with a heterogeneous distribution of distances and cluster sizes. (*b*) Formation of polymerized F-actin causes a significant ($p < 0.05$) increase in R_2. Relaxation times could also be modulated by the ratio of biotinylated to unbiotinylated actin in the sample.

water, because the polymerized actin structure should prevent water from becoming trapped in the middle of the ferritin clusters. There is a possibility that water bound to the surface of actin is experiencing a large dephasing magnetic field. The case of G-actin most likely represents close-packed ferritin in small clusters, which explains why R_2 increased rather than decreased with polymerization in these experiments.

The effects of ferritin aggregation and spacing on relaxivity depend upon the diffusion coefficient of the water, time allowed during the experiment for diffusion through the gradients to occur (interecho spacing), and the distance between the perturbers in the aggregates. Additionally, the amount of iron-loading in the ferritin determines the total signal available at a specific TE, and the distance the magnetic field gradient extends from each molecule. In the simulations presented here, water diffused $\sim 3\ \mu$m during the experiment. This compares to a perturber aggregate diameter range of 65 nm to 1.27 μm in the largest aggregates ($5 \times 5 \times 5$). The peak relaxivity change occurred when this aggregate was 600 nm across. For smaller aggregates, the diameter of the aggregate for peak relaxivity was smaller ($\sim$125 nm with the $2 \times 2 \times 2$ perturbers). We hypothesize that this represents an interplay between two effects: 1), Maximum relaxation for very sparse perturbers, with diffusion distance less than the interperturber distance, occurs when the perturber size is largest. This is seen with the largest aggregates, where the water experiences few perturbers but a very large gradient when it is in the vicinity of the aggregates. 2), When perturbers are less sparse, the water experiences a smaller gradient more often during the experiment, as happens when the aggregates are smaller. As the diffusion coefficient increases, there is expected to be less difference between these two cases. In general, the complicated nature of aggregation suggests that it is appropriate to design a biological construct that is tailored to the microenvironment of the cellular water and the loading factor of ferritin.

An aim of this work was to determine optimal conditions for aggregation of ferritin to improve R_2 relaxivity for MRI. It is instructive to consider whether these small changes in R_2 by ferritin concentration and polymerization status could potentially be detected in vivo. If one assumes some arbitrary threshold for detection of ΔR_2 by ferritin expression, aggregation of the ferritin will thus allow detection at a lower concentration. This threshold is still unclear. We estimate that, given an R_2 relaxivity of 10 mM^{-1}/s, a ferritin subunit concentration of $\sim$200 μM (5-μM cages) is required for a 10% change in signal intensity. Based on the work presented here, perhaps a 100-μM ferritin subunit (2.5-μM cages) concentration could be detected if the ferritin were engineered to aggregate. At this concentration, every ferritin cage would be spaced $\sim$70 nm apart (center-to-center) if uniformly distributed in the entire imaging voxel, demonstrating the high levels of ferritin expression required to be

detectable by MRI. However, it is known that ferritin aggregation occurs to some degree in vivo in the form of hemosiderin (19,20), which would decrease the effect that engineering ferritin aggregates would have.

An alternate and perhaps more interesting implication of this work is that allowing ferritin to alter spacing in a cell can enable reporting on the functional state of different structures. For instance, actin structure is known to change with rapid changes in cellular ion concentrations (30–32), during cell cycle transitions and during cell migration. Producing a ferritin-actin form by ferritin-actin fusion, or by fusion of ferritin to an actin-binding protein, could be used to change spacing between ferritin and to detect actin polymerization states that change on the order of minutes to hours. Other cellular phenomena, such as cell signaling and apoptosis, could potentially be detected by coupling the aggregation of ferritin to proteins that aggregate upon activation. Previous work has proposed controlling the aggregation of iron oxide particles at short distances to make functional MRI contrast agents that report on membrane potentials, enzyme activity, or Ca^{2+} levels (33,36–38). It is not clear yet how to efficiently deliver these agents to cells, or whether the relatively large particles would be able to diffuse through the cell on relevant time scales. Engineering particles to change spacing at relatively short distances ($\approx$50 nm) may offer many advantages for making the aggregation of super-paramagnetic particles a practical strategy for generating functional MRI contrast. Actin is expressed at $\approx$1.5 mg/mL (39) in the cytosol, or at a concentration of $\approx$350 μM. On average, this would require $\sim 3.5 \times 10^7$ actin monomers in a volume of 1 pl, corresponding to the volume of a cell of 10 μm^3. This would suggest that there are 1.5-G-actin monomers per nanometer and that an actin-ferritin fusion must be expressed at a concentration of 10 μM to be spaced at a distance of 50 nm if actin-ferritin is completely dispersed in the cell.

In this work, we have shown how ferritin aggregation can change transverse MR relaxivity. A computational model was developed to determine how the spacing and size of these aggregates affects ΔR_2. The model demonstrates that interparticle spacing within an aggregate on the order of 100 nm modulates R_2. We chemically cross-linked ferritin cages in vitro at short distance, and found that relaxivity was increased by 70% with ferritin aggregates of 100 μm isotropically. We also conjugated ferritin to actin, which was then polymerized to increase R_2 relaxivity by 30%. We hypothesize that the controlled in vivo aggregation of ferritin can be achieved to improve the detectability of gene expression in mammalian cells and binding ferritin to cellular micro-structures, such as the actin cytoskeleton, may be a way to generate MRI contrast from changes in cell function.

S. Cheng and V. Crocker at the National Institute of Neurological Disorders and Stroke Electron Microscopy facility generously provided instruction and assistance with electron microscopy. We appreciate helpful discussions with R. Conroy, J. Sumner, and T. Hu. The authors also thank S. J. Dodd for expert advice and assistance.

This work was supported by the intramural research program, NINDS, National Institutes of Health.

REFERENCES

1. Geninatti, C. S., A. Barge, E. Battistini, C. Cabella, S. Coluccia, D. Longo, V. Mainero, G. Tarone, and S. Aime. 2005. Magnetic resonance imaging visualization of targeted cells by the internalization of supramolecular adducts formed between avidin and biotinylated Gd3+ chelates. *J. Biol. Inorg. Chem.* 10:78–86.
2. Zhang, S., M. Merritt, D. E. Woessner, R. E. Lenkinski, and A. D. Sherry. 2003. PARACEST agents: modulating MRI contrast via water proton exchange. *Acc. Chem. Res.* 36:783–790.
3. Louie, A. Y., M. M. Huber, E. T. Ahrens, U. Rothbacher, R. Moats, R. E. Jacobs, S. E. Fraser, and T. J. Meade. 2000. *In vivo* visualization of gene expression using magnetic resonance imaging. *Nat. Biotechnol.* 18:321–325.
4. Josephson, L., M.F. Kircher, U. Mahmood, Y. Tang, and R. Weissleder. 2002. Near-infrared fluorescent nanoparticles as combined MR/optical imaging probes. *Bioconjug. Chem.* 13:554–560.
5. Lowe, M. P. 2004. Activated MR contrast agents. *Curr. Pharm. Biotechnol.* 5:519–528.
6. Xia, M., V. Kodibagkar, H. Liu, and R. P. Mason. 2006. Tumour oxygen dynamics measured simultaneously by near-infrared spectroscopy and 19F magnetic resonance imaging in rats. *Phys. Med. Biol.* 51:45–60.
7. Gilad, A. A., P. T. Winnard, Jr., P. C. van Zijl, and J. W. Bulte. 2007. Developing MR reporter genes: promises and pitfalls. *NMR Biomed.* 20:275–290.
8. Gottesfeld, Z., and M. Neeman. 1996. Ferritin effect on the transverse relaxation of water: NMR microscopy at 9.4T. *Magn. Reson. Med.* 35:514–520.
9. Cohen, B., H. Dafni, G. Meir, A. Harmelin, and M. Neeman. 2005. Ferritin as an endogenous MRI reporter for noninvasive imaging of gene expression in C6 glioma tumors. *Neoplasia.* 7:109–117.
10. Genove, G., U. DeMarco, H. Xu, W. F. Goins, and E. T. Ahrens. 2005. A new transgene reporter for *in vivo* magnetic resonance imaging. *Nat. Med.* 11:450–454.
11. Deans, A. E., Y. Z. Wadghiri, L. M. Bernas, X. Yu, B. K. Rutt, and D. H. Turnbull. 2006. Cellular MRI contrast via coexpression of transferrin receptor and ferritin. *Magn. Reson. Med.* 56:51–59.
12. Gossuin, Y., R. N. Muller, P. Gillis, and L. Bartel. 2005. Relaxivities of human liver and spleen ferritin. *Magn. Reson. Imaging.* 23:1001–1004.
13. Chasteen, N. D., and P. M. Harrison. 1999. Mineralization in ferritin: an efficient means of iron storage. *J. Struct. Biol.* 126:182–194.
14. Koenig, S. H., D. Brown III, J. F. Gibson, R. J. Ward, and T. J. Peters. 1986. Relaxometry of ferritin solutions and the influence of the Fe^{3+} core ions. *Magn. Reson. Med.* 3:755–767.
15. Bulte, J. M., J. Vymazal, R. A. Brooks, C. Pierpaoli, and J. A. Frank. 1993. Frequency dependence of MR relaxation times. II. Iron oxides. *J. Magn. Reson. Imaging.* 3:641–648.
16. Hilty, S., B. Webb, R. B. Frankel, and G. D. Watt. 1994. Iron core formation in horse spleen ferritin: magnetic susceptibility, pH, and compositional studies. *J. Inorg. Biochem.* 56:173–185.
17. Brooks, R. A., J. Vymazal, R. B. Goldfarb, J. M. Bulte, and P. Aisen. 1998. Relaxometry and magnetometry of ferritin. *Magn. Reson. Med.* 40:227–235.
18. Gossuin, Y., A. Roch, R. N. Muller, P. Gillis, and F. Lo Bue. 2002. Anomolous nuclear magnetic relaxation of aqueous solutions of ferritin: an unprecedented first-order mechanism. *Magn. Reson. Med.* 48:959–964.
19. Stark, D. D., N. M. Bass, A. A. Moss, B. R. Bacon, J. H. McKerrow, C. E. Cann, A. Brito, and H. I. Goldberg. 1983. Nuclear magnetic resonance imaging of experimentally induced liver disease. *Radiology.* 148:743–751.
20. Gossuin, Y., C. Burtea, A. Monseux, G. Toubeau, A. Roch, R. N. Muller, and P. Gillis. 2004. Ferritin-induced relaxation in tissues: an *in vitro* study. *J. Magn. Reson. Imaging.* 20:690–696.

21. Meldrum, F. C., B. R. Heywood, and S. Mann. 1992. Magnetoferritin: in vitro synthesis of a novel magnetic protein. *Science*. 257:522–523.

22. Bulte, J. W., T. Douglas, S. Mann, R. B. Frankel, B. M. Moskowitz, R. A. Brooks, C. D. Baumgarner, J. Vymazal, M. P. Strub, and J. A. Frank. 1994. Magnetoferritin: characterization of a novel superparamagnetic MR contrast agent. *J. Magn. Reson. Imaging*. 4:497–505.

23. Weisskoff, R. M., C. S. Zuo, J. L. Boxerman, and B. R. Rosen. 1994. Microscopic susceptibility variation and transverse relation: theory and experiment. *Magn. Reson. Med.* 31:601–610.

24. Jensen, J. H., and R. Chandra. NMR relaxation in tissues with weak magnetic inhomogeneities.2000. *Magn Reson Med.* 44:144–156.

25. Jensen, J. H., R. Chandra, and H. Yu. 2001. Quantitative model for the interecho time dependence of the CPMG relaxation rate in iron-rich gray matter. *Magn. Reson. Med.* 46:159–165.

26. Wood, J. C., J. D. Fassler, and T. Meade. 2004. Mimicking liver iron overload using liposomal ferritin preparations. *Magn. Reson. Med.* 51: 607–611.

27. Frank, S., and P. C. Lauterbur. 1993. Voltage-sensitive magnetic gels as magnetic resonance monitoring agents. *Nature*. 363:334–336.

28. Bogdanov, A., Jr., L. Matuszewski, C. Bremer, A. Petrovsky, and R. Weissleder. 2002. Oligomerization of paramagnetic substrates results in signal amplification and can be used for MR imaging of molecular targets. *Mol. Imaging*. 1:16–23.

29. Steinmetz, M. O., K. N. Goldie, and U. Aebi. 1997. A correlative analysis of actin filament assembly, structure, and dynamics. *J. Cell Biol.* 138:559–574.

30. Goldmann, W. H. 2002. Examination of actin polymerization and viscosity induced by cations and ionic strength when cross-linked by alpha-actinin. *Cell Biol. Int.* 26:541–546.

31. Lange, K., and J. Gartzke. 2006. F-actin-based Ca signaling—a critical comparison with the current concept of Ca signaling. *J. Cell. Physiol.* 209:270–287.

32. Nusco, G. A., J. T. Chun, E. Ercolano, D. Lim, G. Gragnaniello, K. Kyozuka, and L. Santella. 2006. Modulation of calcium signaling by the actin-binding protein cofilin. *Biochem. Biophys. Res. Commun.* 348: 109–114.

33. Atanasijevic, T., M. Shusteff, P. Fam, and A. Jasanoff. 2006. Calcium-sensitive MRI contrast agents based on superparamagnetic iron oxide nanoparticles and calmodulin. *Proc. Natl. Acad. Sci. USA*. 103:14707–14712.

34. Danon, D., L. Goldstein, Y. Marikovsky, and E. Skutelsky. 1972. Use of cationized ferritin as a label of negative charges on cell surfaces. *J. Ultrastruct. Res.* 38:500–510.

35. Mikawa, M., H. Kato, M. Okumura, M. Narazaki, Y. Kanazawa, N. Miwa, and H. Shinohara. 2001. Paramagnetic water-soluble metallofullerenes having the highest relaxivity for MRI contrast agents. *Bioconjug. Chem.* 12:510–514.

36. Bogdanov, A. A., C. Martin, R. Weissleder, and T. J. Brady. 1994. Trapping of dextran-coated colloids in liposomes by transient binding to aminophospholipid: preparation of ferrosomes. *Biochim. Biophys. Acta*. 1193:212–218.

37. Wunderbaldinger, P., L. Josephson, and R. Weissleder. 2002. Cross-linked iron oxides (CLIO): a new platform for the development of targeted MR contrast agents. *Acad. Radiol.* 9(Suppl. 2):304–306.

38. Josephson, L., M.F. Kircher, U. Mahmood, Y. Tang, and R. Weissleder. 2002. Near-infrared fluorescent nanoparticles as combined MR/optical imaging probes. *Bioconjug. Chem.* 13:554–560.

39. Merriam, R. W., and T. G. Clark. 1978. Actin in Xenopus oocytes. II. Intracellular distribution and polymerizability. *J Cell Biol.* 77: 439–447.